

Terrestrial-style slow-moving earthflow kinematics in a submarine landslide complex

Joshu J. Mountjoy^{a,b,*}, Jim McKean^c, Philip M. Barnes^a, Jarg R. Pettinga^b

^a National Institute of Water and Atmospheric Research Ltd, Private Bag 14901, Wellington, New Zealand

^b Dept. of Geological Sciences, University of Canterbury, Private Bag 4800, Christchurch, New Zealand

^c USDA Forest Service, 322 E. Front Street, Boise, ID 83702, United States

ARTICLE INFO

Article history:

Received 17 March 2009

Received in revised form 2 September 2009

Accepted 5 September 2009

Available online 5 October 2009

Communicated by D.J.W. Piper

Keywords:

submarine earthflow
mass transport complex
morphometric analysis
landslide kinematics
EM300 multibeam
submarine geomorphology

ABSTRACT

Morphometric analysis of Simrad EM300 multibeam bathymetric DEMs reveals details of deformation patterns in a ~145 km² submarine landslide complex that are commonly associated with slow-moving earthflows in terrestrial settings. This mode of failure, where existing landslide debris is remobilised repeatedly along discrete shear boundaries and is progressively conveyed through the complex, has not previously been recognised in the submarine environment. The kinematics contrast with the more traditional models of submarine landslide complex development in which repeated catastrophic failures each mobilise new source material to form a composite stacked landslide deposit. In our study of the Tuaheni landslide complex on the Hikurangi Margin of New Zealand, remobilisation has formed boundary shear zones imaged at the seafloor surface in multibeam data, and at depth in multichannel seismic reflection data. A significant amount of internal deformation has occurred within the debris streams. Phases of deformation appear to be partitioned longitudinally as extensional and contractional zones rooted into a basal decollement, and laterally with strike-slip shears partitioning discrete debris streams. While slow-moving terrestrial earthflows are activated by fluctuating piezometric levels typically controlled by precipitation, different processes cause the equivalent mobility in a submarine earthflow. Elevated pore pressures in submarine earthflows are produced by processes such as earthquake-generated strong ground motion and/or gas/fluid release. Earthflow movement in submarine settings is prolonged by slow dissipation in pore pressure.

© 2009 Elsevier B.V. All rights reserved.

1. Introduction

Detailed characteristics of submarine landslide morphologies are ever more apparent with increasing resolution of multibeam bathymetry and 3D seismic imaging technologies (e.g. Greene et al., 2006; Gee et al., 2007; Micallef et al., 2007a). Failure modes of submarine landslides vary from translational and rotational movements of relatively intact slide masses, to fluidised flows which may involve a wide range of material from hard rock to underconsolidated sediment (e.g. Mulder and Cochonot, 1996; Hampton et al., 1996). Traditionally, the development of submarine landslide complexes is modelled as repeated failures mobilising new source material with each event, with the landslide debris either accumulating in the same depositional area where slope gradient decreases (Fig. 1A), or being repetitively flushed through a channelized system (e.g. Canals et al., 2004). In this representation, slopes fail catastrophically and slide material is only

mobilised once. Ages of submarine landslides are generally determined using stratigraphic dating techniques (e.g. Evans et al., 2005), based on this conceptual model for the development of landslide complexes.

Terrestrial hillslopes also host a variety of catastrophic “event” style failures such as falls, slides and flows (Varnes, 1978; Cruden and Varnes, 1996) that involve the original mass instability of previously unfailed material. In addition, however, landslide complexes in areas of weak, clay-bearing rock can behave as slow, glacier-like debris streams that repeatedly remobilise the same material and are generally referred to as either earthflows (Hungri et al., 2001; Baum et al., 2003) or mudslides (Hutchinson, 1988; Picarelli et al., 2005; Glastonbury and Fell, 2008). The two terms refer to the same process (Hungri et al., 2001), and in this paper we will use the term earthflow or slow-earthflow.

Despite the identification of numerous slope failure modes that are common to subaerial and submarine settings, earthflow-type failures have not been documented on submarine slopes. We propose that earthflows do occur in the submarine environment and, that while they have very similar morphological characteristics to slow-moving terrestrial earthflows, they exhibit some important mechanical differences and are subject to different triggering mechanisms (Fig. 1C–F).

* Corresponding author. National Institute of Water and Atmospheric Research Ltd, Private Bag 14901, Wellington, New Zealand. Tel.: +64 4 3860336.

E-mail address: J.Mountjoy@niwa.co.nz (J.J. Mountjoy).

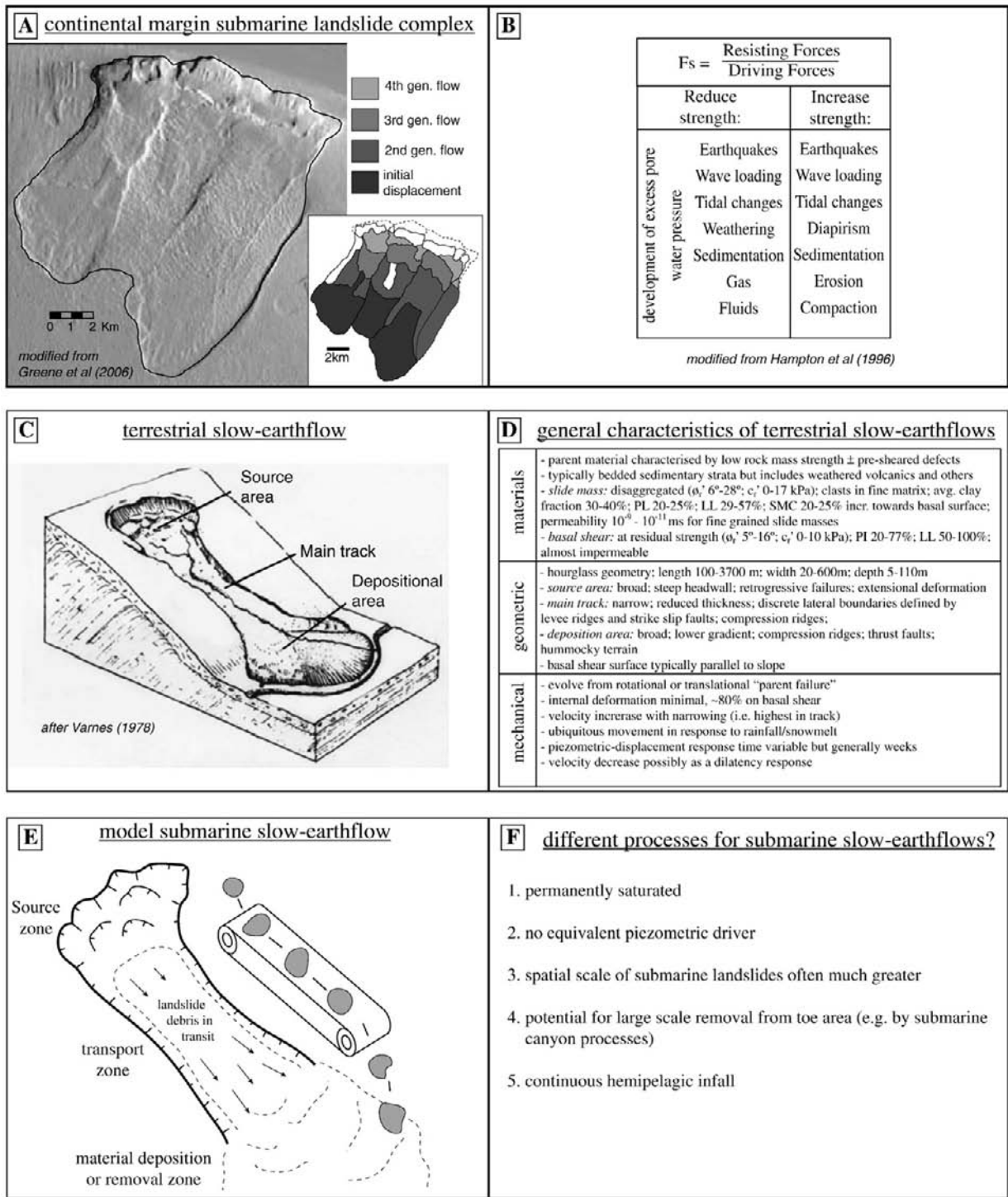


Fig. 1. A) The Goleta landslide. The landslide complex is formed by multiple discrete slope failure events (Greene et al., 2006). B) Controlling factors in the stability of a submarine slope in terms of a simple Factor of Safety (F_s) equation; and tabulated processes that increase and decrease slope strength. C) Schematic diagram of an active slow-moving terrestrial earthflow. D) Fundamental characteristics from a variety of case study earthflows (Hungry et al., 2001; Baum et al., 2003; Glastonbury and Fell, 2008). E) Generalised schematic model proposed for a submarine earthflow as a "conveyor belt" progressively transporting material from a source area to a depositional area. F) Contrasting factors for submarine vs terrestrial earthflows.

A newly mapped submarine landslide complex on the upper continental slope of the Hikurangi subduction margin of New Zealand, referred to here as the Tuaheni landslide complex, has morphological characteristics of a slow-moving earthflow. These features are revealed by Simrad EM300 multibeam bathymetric data and multi-channel seismic reflection profiles, allowing detailed resolution of surface and subsurface character. In this paper we: 1) analyse the

three dimensional geometry of this landslide complex; 2) consider the kinematic behaviour of the landslide; and, 3) present a conceptual model of repeated failure in a submarine earthflow complex. Earthflows are persistently active landslides that move on seasonal to decadal and longer timescales. The main landslide body acts as a conveyor for material from the source area at the head of the slide and moves debris downslope through a transport zone or "track" to the

depositional lobe and toe area (Fig. 1C and D). Mechanical movement of material through the transport zone is primarily (~80%) accomplished by displacement on lateral and basal shear surfaces/zones with a component of quasi-brittle deformation in the main landslide body (Fleming and Johnson, 1989; Hungr et al., 2001; Parise, 2003; Baum et al., 2003; McKean and Roering, 2004; Picarelli et al., 2005; Bertolini and Pizzolo, 2008). In the majority of subaerial slope failures, (re)activation of earthflows is predominantly triggered by elevated pore pressures accompanying a piezometric rise in the landslide body principally as a result of precipitation; but also in response to other mechanisms including earthquakes, snow melt and lateral groundwater inflow (Glastonbury and Fell, 2008; Bertolini and Pizzolo, 2008).

In contrast to the dominant role that precipitation plays in subaerial slope instability, no equivalent dominant trigger has been identified for submarine slope instability, with landslides initiating in response to a range of processes (e.g. Hampton et al., 1996; Locat and Lee, 2002) (Fig. 1B). While gravity is obviously a first-order effect on submarine slopes, it is typically other factors such as earthquake ground motion, gas expulsion and sediment loading that ultimately trigger slope failure, predominantly through the development of excess pore pressure.

Landslides can be distinguished from unfailed hillslopes by characteristic morphological features such as scarps and hummocky terrain (Cruden and Varnes, 1996), and in a more regional context by the scale of surface roughness of the landslide deposit (McKean and Roering, 2004; Glenn et al., 2006). Furthermore, the failure mode and mechanical behaviour of an individual landslide may be characterised by surface morphology reflecting behaviour of the landslide body at depth. For example, bedrock translational and rotational failures commonly have broad, steep head scarps and mid-slope benches reflecting the disruption of intact bedrock blocks within the slide mass (Cruden and Varnes, 1996). In contrast, earthflow morphology is characterised by: 1) deflation in the main landslide “track” (Picarelli et al., 2005); 2) lateral shear boundaries manifested as discrete shear zones or en-echelon cracks (Baum et al., 2003); and 3) extensional deformation features in the source area and compressional deformation features in the lower track and toe area (Glastonbury and Fell, 2008). Additionally, landslide features developed by multiple overlapping flow-like events (e.g. Fig. 1A) would be obliterated by repeated debris deformation in an earthflow. Given that submarine landslides are, as a matter of necessity primarily studied using remote sensing techniques, it is important to be able to investigate their kinematic behaviour from morphological characteristics.

2. Regional setting

The Tuaheni landslide complex (TLC) is located on the upper slope of the Hikurangi Margin, off the east coast of the North Island of New Zealand (Fig. 2A). Active subduction of the Pacific Plate under the Australian Plate occurs with an oblique convergence rate of ~46 mm/year (Beavan et al., 2002). Active eastward verging splay faults from the plate boundary mega-thrust project to the seafloor on the lower slope and across the continental shelf (Barker et al., 2009). On the mid- to upper slope, where this study is focused, there is a paucity of currently active structures, and the active fault most proximal to the landslide is the Ariel Bank Fault (Fig. 2B). To the south the Ariel Bank Fault steps over to the Lachlan Fault, which has a late Quaternary displacement rate of 3.0–6.5 mm/year (Barnes et al., 2002). Preliminary analysis shows that the rate of activity of both faults is similar. Probabilistic seismic hazard modelling of regional earthquake sources shows that peak ground accelerations (PGA) of the order of 0.3–0.4 g occur at a 475 year return time and, of the order of 0.5–0.6 g at a 1000 year return time (Stirling et al., 2002). Some moderately large magnitude historic earthquakes have occurred in the vicinity, the largest of which was the 1931 M7.8 Napier

earthquake some 130 km to the southwest, and more recently in 2007 the M6.8 Gisborne earthquake with the epicentre within the study area, with a focal depth of ~44 km.

The TLC occurs within muddy sedimentary deposits that accumulated primarily during periods of eustatic sea level lowering (Fig. 2C) (c.f. Lewis et al., 2004; Paquet et al., 2009). These deposits extend off-shelf onto the upper slope, and form a wedge shaped, gently dipping, parallel bedded sedimentary package (i.e. lowstand systems tract or lowstand wedge) that is well imaged in multichannel seismic data (Fig. 2C). 3.5 kHz seismic reflection data reveal a parallel stratified section in the upper ~50 m, in close agreement with a relatively undisturbed seafloor depositional surface, and characteristic of a Holocene hemipelagic succession (e.g. Carter and Manighetti, 2006) overlying the lowstand wedge. Geotechnical testing of similar sedimentary deposits on the upper slope to the south show that there is little variation between the character of underlying lowstand deposits and post-glacial sediment drape (Barnes et al., 1991). Results from Barnes et al. (1991) showed that average grainsize distribution is ~2% sand, ~53% silt and ~45% clay; with the clay fraction composed of smectite (24–47%), illite (23–34%) and chlorite (20–24%); and the Plasticity Index ranging from 34 to 50%. Residual strength from ring shear test on two samples found internal friction angles of 19.5–22.5°. These values are likely to be roughly applicable to the material within the TLC. No active fault or fold structure is mapped directly beneath the sedimentary wedge within which the Tuaheni landslide complex occurs, and the sequence does not appear to have experienced any post-depositional tectonic deformation.

3. Data and methodology

This study is primarily based on 30 kHz multibeam bathymetric data collected with a SIMRAD EM300 multibeam system mounted on the hull of New Zealand's National Institute of Water and Atmospheric Research (NIWA) ship *RV TANGAROA*. The system operates 135 $1 \times 2^\circ$ beams at 30 kHz frequency. Shipboard navigation comprises a POS/MV system with differential GPS. Surveys were conducted in 2001 (Tan0106), 2006 (Tan0616) and 2008 (Tan0810). The relevant part of the multibeam data set spans water depths of 150–900 m and a grid size of 25 m is chosen to honor beam insonification and sounding density across these water depths. Data were processed to this resolution in Hydromap. High resolution data are augmented with a regional 100 m bathymetric grid built from a combination of 12 kHz SIMRAD EM12Dual multibeam data collected aboard *RV L'ATALANTE* in the early 1990s, and single beam echo sounder bathymetric data held in the NIWA database.

Two multichannel seismic reflection (MCS) datasets are presented in this study: 1) *RV TANGAROA* 2001 (TAN0106) 6 fold, 24-channel seismic profiles acquired with a GI gun source in 45/105 mode; and, 2) *MV PACIFIC TITAN* 2005 (CM05) up to 960-channel high fold 2D seismic reflection data recorded to 12 second TWT (Multiwave, 2005; Barker et al., 2009).

High resolution 3.5 kHz data are available from all *RV TANGAROA* multibeam cruises undertaken in the study area as well as additional data from NIWA archives.

3.1. Objective surface-feature delineation methodology

The surface roughness of landslide debris has been delineated using digital elevation models (DEMs) in terrestrial (McKean and Roering, 2004; Glenn et al., 2006), and submarine settings (Micallef et al., 2007a; Micallef et al., 2007b). McKean and Roering (2004) successfully applied 1-D, circular (2-D) and spherical (3-D) statistics to an airborne lidar-derived DEM, mapping both the location and extent of a terrestrial earthflow, as well as geomorphic detail on the landslide surface. The technique quantifies the degree and pattern of dispersion of unit vectors constructed normal to each grid cell in a DEM (Fig. 3A). Their spherical

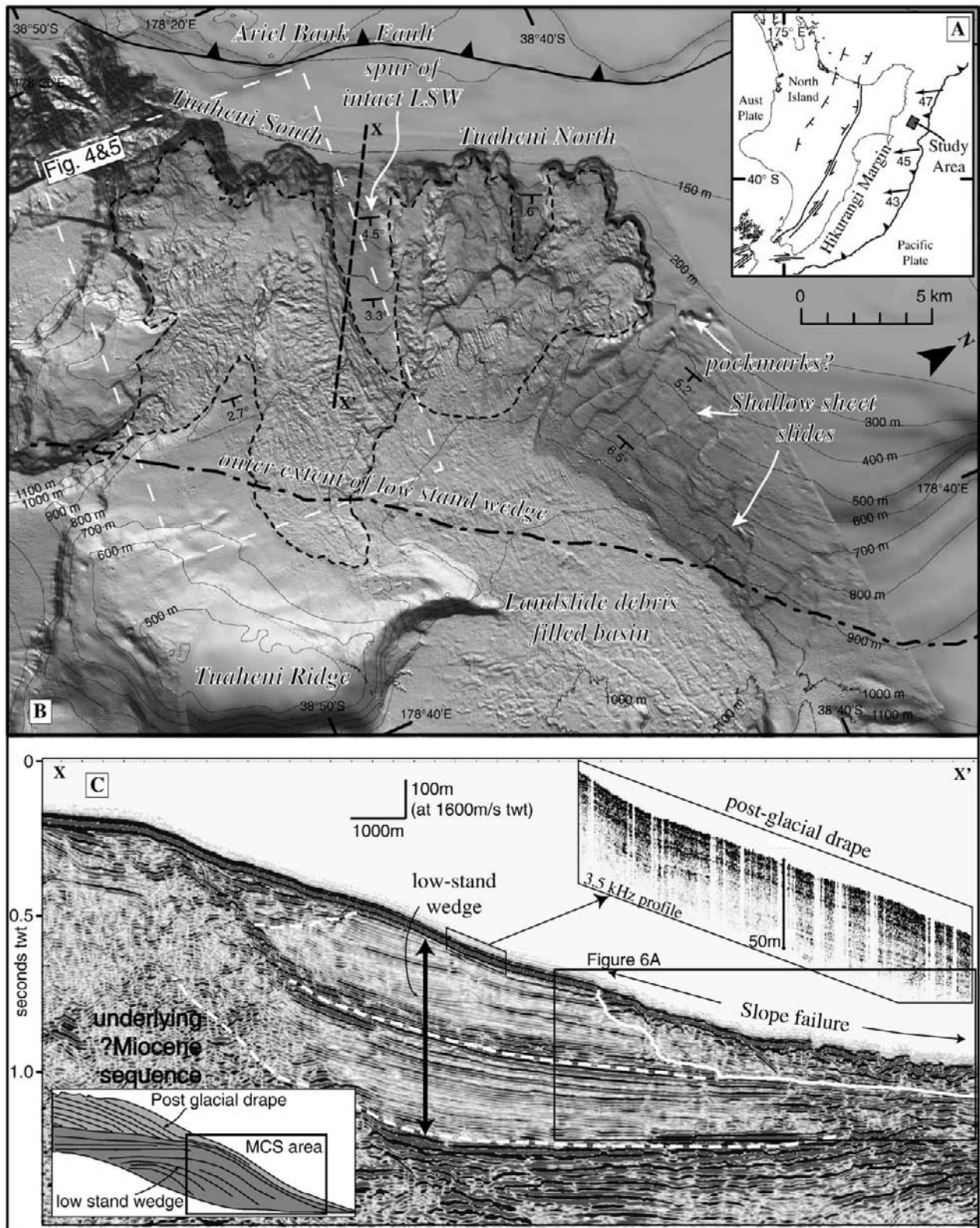


Fig. 2. A) Tectonic setting of New Zealand's North Island east coast showing the principal tectonic elements and plate convergence direction and rates (after Beavan et al., 2002). The study area is located within the grey box. B) Shaded relief map showing the Tuaheni landslide complex (TLC) on the upper continental slope. The two components of the TLC, Tuaheni South and Tuaheni North, are outlined in black dashed lines. The outer (off-shelf) extent of the lowstand wedge (LSW), as imaged in C, is shown by the black dash-dot line. C) Multichannel seismic profile X-X' (located in 2B) illustrating the lowstand sedimentary deposit within which the TLC occurs. The white dashed lines indicate the base of, and a possible sequence boundary within, the sedimentary body. The solid white line defines the basal extent of landslide debris. The inset line drawing shows the simple lowstand systems tract model (after Posamentier and Vail, 1988). A 3.5 kHz seismic profile is presented to illustrate the undeformed nature of the hemipelagic accumulation on the upper sequence. The vertical data gaps are a result of acoustic bubble noise below the survey vessel.

method was used in this study because it considers local changes in both slope and aspect of the ground surface, while the 1- and 2-D methods use only one or the other of these topographic attributes.

The spherical statistic is calculated from the ratios of normalized eigenvalues of the orientation matrix of the unit vectors in an area of a DEM. These ratios can describe not only the degree of variability in vector orientations, but also if there is pattern in the orientations. Here we restrict our analysis to the ratio of the first and second eigenvalues, which describe the degree of clustering of the vectors (see Fig. 3B, the ratio $\ln(S1/S2)$). The spherical statistics analysis is made in a square window of DEM cells and then that local value of $\ln(S1/S2)$ is assigned to the central cell in the window. By moving the sampling window over a DEM as the calculation is repeated, the elevation matrix is remapped as the local topographic surface roughness. The roughness defined by $\ln(S1/S2)$ over some area of a DEM is a function of both the degree of local variability in slope and aspect and the distance over which the variation occurs. This spatial scaling can be evaluated by changing the size of the sampling window; an increase in sample window size gives a larger vector population across which clustering patterns are analysed. For a more detailed description of the technique the reader is referred to McKean and Roering (2004). In this study we refer to the methodology as the “spherical statistics” technique.

4. Results: the Tuaheni landslide complex

Much of the upper slope above Tuaheni Ridge exhibits significant bathymetric surface roughness at 10–100 m length scales and has a surface morphology indicative of mass movement. This area is referred to as the Tuaheni landslide complex (TLC) (Fig. 2B). Likewise in MCS data the mass movements cause highly chaotic reflectivity, characteristic of slope failure debris, in comparison to adjacent apparently unfailed material with well developed bedding (Fig. 2C). The ~145 km² landslide complex is divided into two domains; Tuaheni North and Tuaheni South, separated by a ~2 km wide spur of smooth unfailed seafloor (line X–X' Fig. 2B). Sharply curved head scarps define individual component failures that initiate at the shelf-edge to upper-slope transition at ~150 m water depth. These arcuate failures collectively affect a ~20 km length of the upper slope. The individual scarp heights in the source area are variable, ranging from c. 300 m in the south and decreasing to c. 100 m in the north. Debris fans extend out from head scarp areas, and landslide toe areas occur in

water depths of 750–900 m. Beyond the TLC to the southeast bathymetry shallows to less than 500 m on Tuaheni Ridge (Fig. 2B). Slopes adjacent to the TLC have gradients in the range of 2.5–6.5°, while the slope gradient on the surface of the landslide debris within the TLC is lower, with gradients of 1.5–4° in Tuaheni South and 3.5–4° in Tuaheni North.

Along slope to the south of the TLC, slopes are incised by gully systems; while to the east, the slope is generally smooth but does exhibit several subdued scarps up to 30 m high aligned down the slope (Fig. 2B). Circular “pockmarks” occur near the head of these scarps. At the toe of this slope, and to the north and northeast of Tuaheni Ridge there is a sedimentary basin with a >250 ms (~200 m at 1600 ms) thick sequence characterised by chaotic reflectivity in MCS data, and irregular surface roughness in bathymetry data (Fig. 2B).

The basal surface of the landslide debris in Tuaheni South is coincident with the well formed parallel stratification of the lowstand wedge sequence (Fig. 2C). The outer extent of the lowstand wedge was mapped from MCS profiles and underlies the entire TLC area, as well as the slope to the east. Observation in several MCS profiles shows that the relatively undisturbed surface of the lowstand wedge is sub-parallel to bedding (e.g. Fig. 2C main profile and 3.5 kHz inset), and it is apparent from this relationship that the dip of the lowstand wedge strata increases to the N/NE (Fig. 2B).

There are primary differences in the morphology of the Tuaheni North and Tuaheni South components of the TLC. The shelf break head scarp area of Tuaheni North has a complex “scaloped” morphology, with individual scallops between 700 m and 1800 m across. The heights of scarps are predominantly around 100 m, sloping at approximately 8–20°. Tuaheni North contains multiple arcuate scarps through the central part of the landslide debris area. In contrast to Tuaheni North, the surface character of the main debris body of Tuaheni South is totally composed of large areas of irregular, rough landslide debris and does not contain internal scarps similar to those in Tuaheni North. The shelf break area of Tuaheni South is characterised by larger scallops >2500 m wide, 300–350 m high sloping at 8–20°.

We focus on Tuaheni South for morphometric analysis of landslide surface roughness. The landslide debris in Tuaheni South does not exhibit the clear, first-order geomorphic features seen within Tuaheni North (e.g. arcuate scarps), but contains subtle features that require detailed interpretation afforded by roughness-based analysis (e.g. the spherical statistics technique).

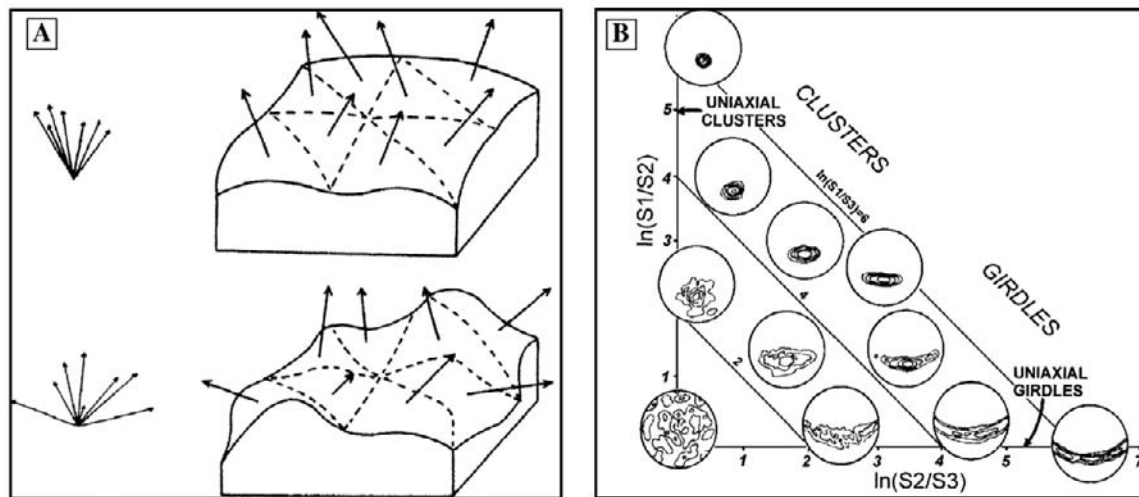


Fig. 3. The eigenvalue-based spherical statistics analysis technique. A) Unit direction vector orientation showing a smooth surface with minimal variations in orientation, and a rough surface with increased variations in orientation (modified from Hobson, 1972). B) Ratios of normalized eigenvalues for analysing vector orientations (modified from Woodcock, 1977).

4.1. Tuaheni South landslide debris roughness characteristics

Tuaheni South contains a $\sim 80 \text{ km}^2$ area of landslide debris. Debris thickness varies between 90 and 135 m (based on available MCS depth conversion assuming a velocity of 1600 m/s, e.g. Fig. 2C), yielding a total debris volume of $10 \pm 0.1 \text{ km}^3$. The (re)activation and movement of a landslide deposit is typically accompanied by internal

structural style deformation (compressional, shear and extensional faulting and associated folding) forming ridges and scarps that can be used to characterise landslide kinematics (Baum et al., 1998; Parise, 2003). The spherical statistics technique has been applied at different scales to map both local and regional scale patterns of deformation by adjusting the sampling window relative to the scale of the topography.

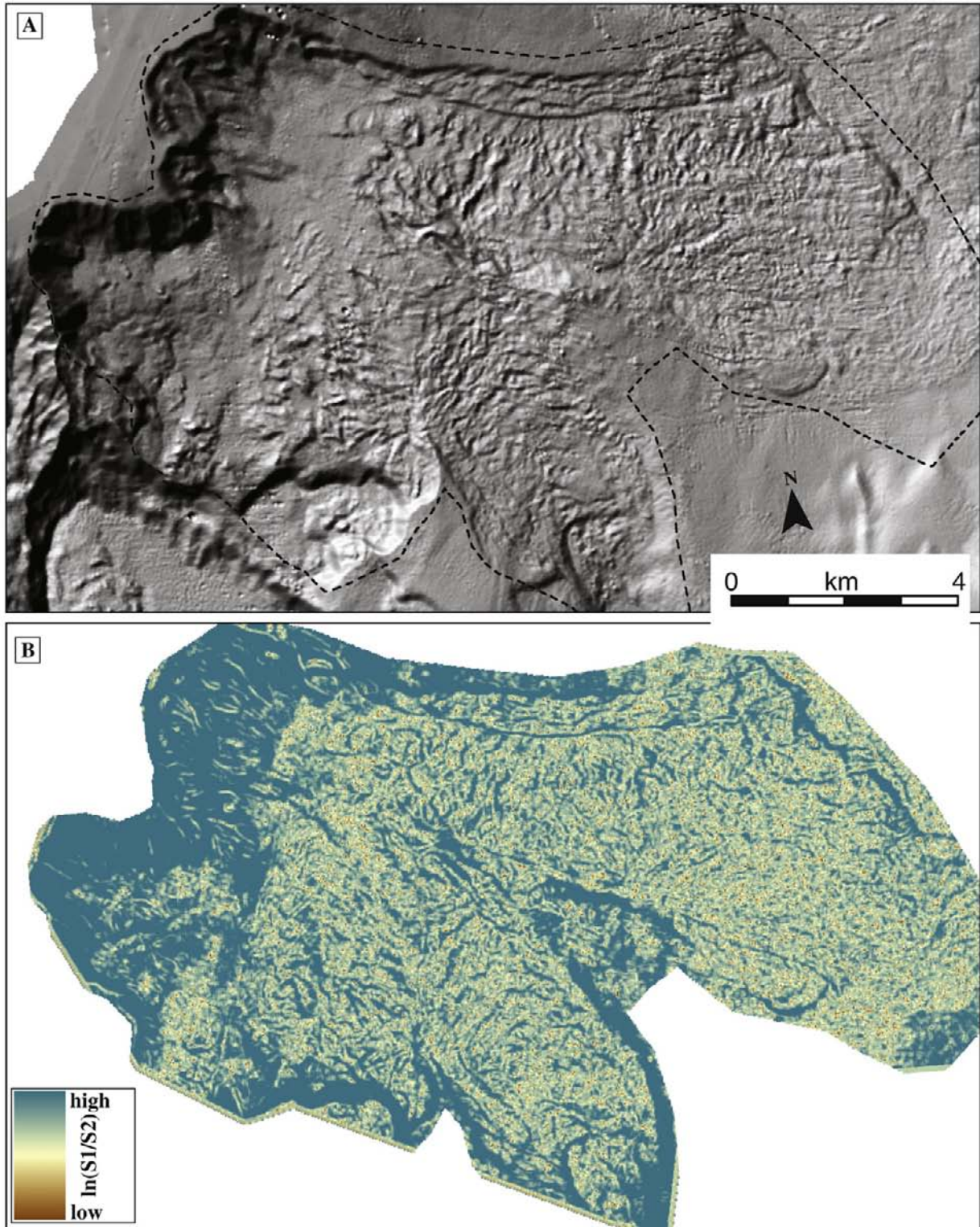


Fig. 4. Roughness characterisation of Tuaheni South (location in Fig. 2B). A) Shaded relief map of the 25 m DEM used for spherical statistics analysis. B) Spherical statistics analysis results ($\ln S1/\ln S2$) from $75 \times 75 \text{ m}$ roaming window for the Tuaheni South landslide complex.

4.1.1. Local-scale spherical statistics analysis

Using the 25 m DEM from survey Tan0810, a 3×3 cell window is applied to Tuaheni South (Fig. 4A). At this 75×75 m scale, the spherical statistics technique isolates internal features within the debris, defining ridge crests as rough (dispersed vectors, low eigenvalues, light colours) and the sloping fronts of ridges and scarps as smooth (clustered vectors, high eigenvalues, dark colours). Minor areas of noise in the data do not significantly affect the analysis. The results of the spherical statistics analysis are incorporated in a GIS where a classified eigenvalue map is used to define roughness elements and assist with mapping surface features within the landslide area (Fig. 5).

Three separate areas of landslide debris are defined, delineated as debris bodies T1, T2 and T3. Debris bodies T2 and T3 have longitudinal scarps along their lateral boundaries, and MCS data show that these features persist at depth (Fig. 6A).

The most well formed example of these lateral scarps is on the northern margin of debris body T3 (Fig. 5), with a 6.5 km-long continuous scarp between 10 and 20 m high. MCS data show a clear reflector, coincident with the scarp base, projecting ~ 95 m below the seafloor at $\sim 26^\circ$ (geometrically derived true dip) (Fig. 6A). Along the length of the scarp, there is a change in strike from 107° to 089° as the debris stream widens from 1.8 to ~ 5.0 km at the toe of the failure (Fig. 5). Upslope or north of the main lateral shear, a less well defined scarp correlates to a reflector in MCS dipping at $\sim 34^\circ$. Widespread failure scarps occur on across the northern-margin slope of the landslide. Other lateral scarps occur on the southern margin of debris body T3, and on both margins of debris body T2. Several linear scarp features occur within the T3 debris body toe area, aligned sub-parallel to the lateral scarps. We note a broad, diffuse reflector in MCS data, towards the base of the chaotic reflectivity (Fig. 6A).

4.1.2. Regional scale spherical statistics analysis

To map regional patterns of debris deformation, we make the assumption that larger scale (amplitude and wavelength) surface features are indicative of localised internal deformation within the

landslide debris. Conceptually, if an area of a relatively smooth debris body deforms in either compression or extension then surface deformation features reflecting internal deformation (folds and/or extensional scarps, e.g. Fig. 6) would differentiate this area from the rest of the landslide debris body.

We have tested a range of increasing roaming window scales to determine which most efficiently distinguishes zones of larger scale surface features, and a 15×15 cell window (375×375 m) best maps larger regional features (Fig. 7). At the upper end of the landslide, the large slopes of the head scarp area are predominantly characterised by a high eigenvalue (orange). Across the three landslide debris bodies T1, T2 and T3 (Figs. 5 and 7B), areas of larger scale surface roughness are delineated as patchy areas of higher eigenvalues (green to orange colours, Fig. 7A).

5. Discussion

The landslide debris of Tuaheni South exhibits numerous features that provide information on kinematic behaviour. Interpretation of surface roughness analysis and MCS data (Figs. 5 and 6) defines numerous features that result from deformation of the debris body, including: 1) areas of compression defined by ridges reflecting compressional deformation correlated to reverse fault-style deformation; 2) areas of extension defined by concave downslope fissures, local sediment accumulation, and dislocated bathymetric features correlated to internal extensional deformation; 3) laterally bounding scarps that project to depth as well formed shear planes; 4) internal longitudinal shears within the toe area of debris body T3; and 5) a possible decollement zone or basal shear in the lower landslide debris. From these features we interpret the movement directions of the debris (the three identified debris bodies T1–T3 Fig. 5). Based on the prominent lateral scarps, and the deflation and lower slope angles of the landslide debris, there has been a large amount of material removed from the landslide scar (e.g. $\sim 2.3 \pm 0.5 \times 10^9 \text{ m}^3$ for the debris body T3 area alone). The geomorphic interpretation can also be used to constrain the style of mass movement at this site.

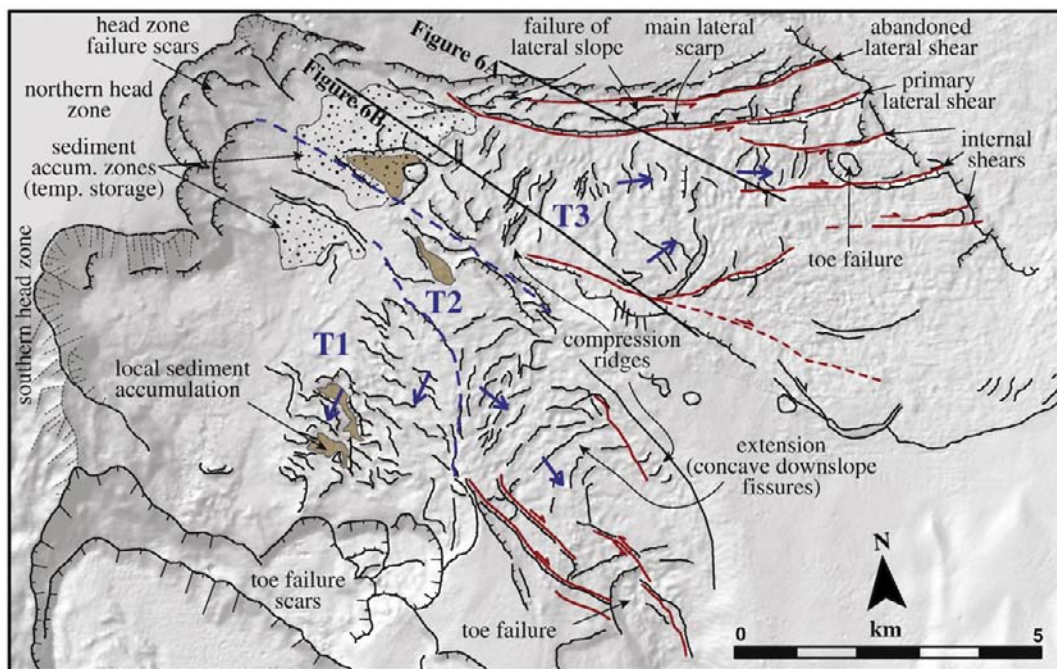


Fig. 5. Geomorphic interpretation of the Tuaheni South landslide complex based on interpretation of surface roughness patterns (see Fig. 4B) and shadowing in the shaded relief model (Fig. 4A). The boundaries of the three discrete earthflow debris bodies (T1–T3) are indicated by blue dashed lines and inferred directions of movement are shown by the blue arrows. Red linework delineates lateral shear zones. Black linework within the landslide bodies maps out internal deformation.

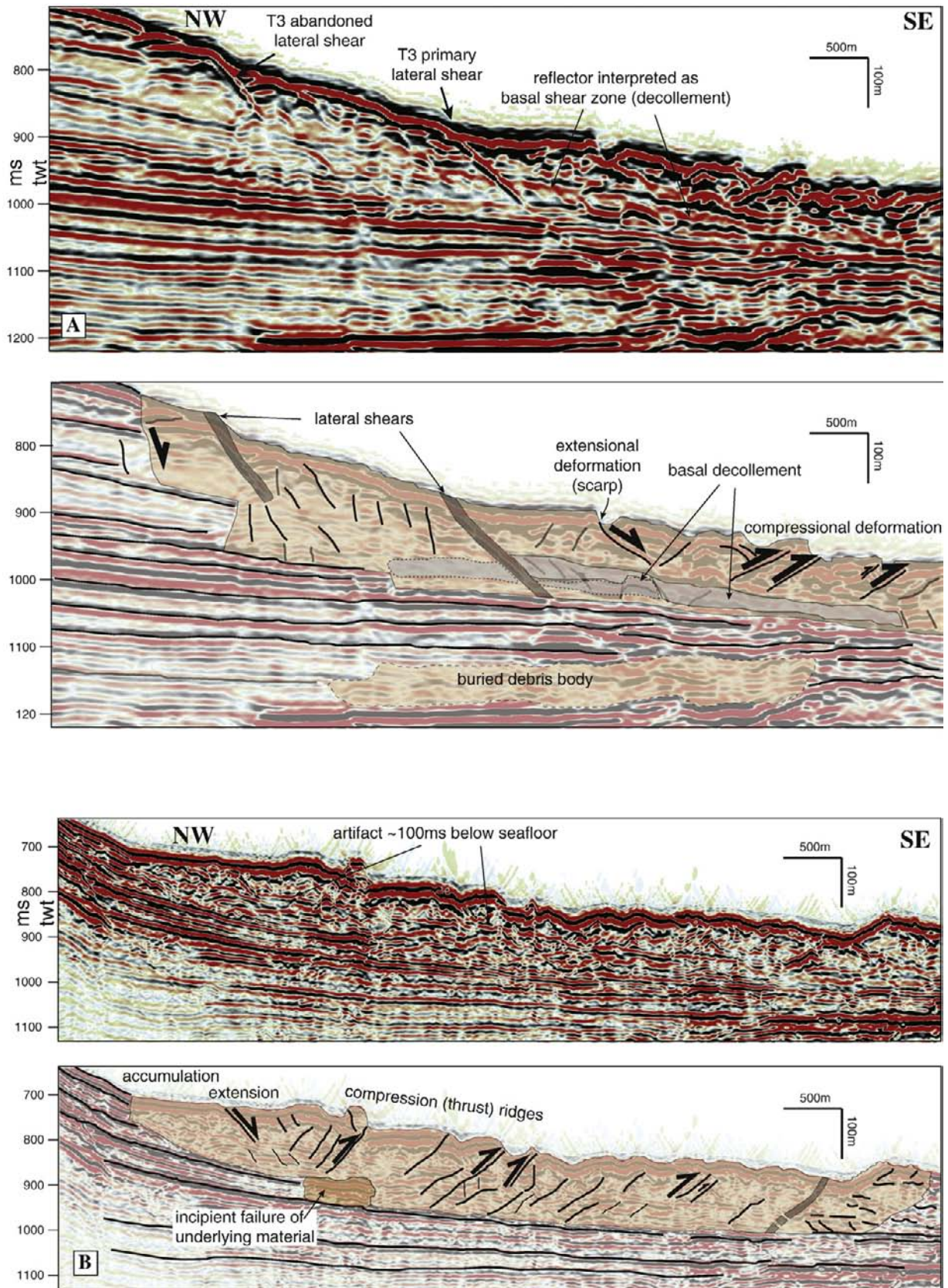


Fig. 6. Uninterpreted and interpreted MCS profiles illustrating subsurface landslide features including lateral shear zones and deformation structures. See Fig. 5 for profile locations. A) 05CM-02. B) Tan 0106-13. The annotated artefact is also clearly observed at ~100 ms below the seafloor in the same profile further to the southeast (not presented here). It is unclear what causes this artefact but, based on its continuation across multiple material types to the southeast, it is clearly not a horizon within the landslide debris.

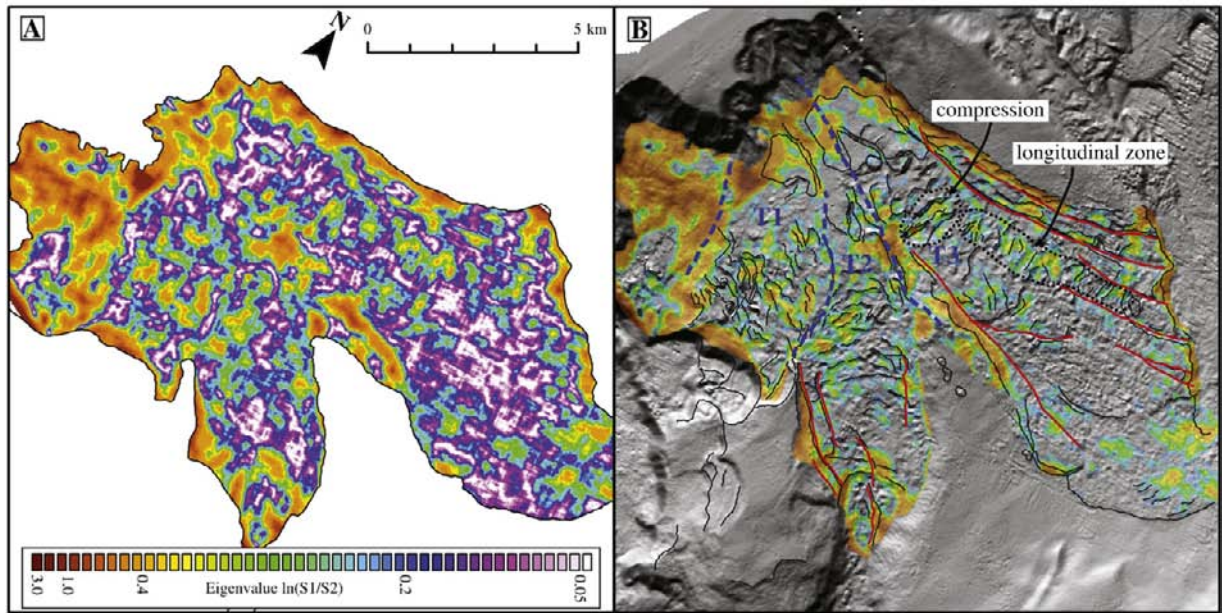


Fig. 7. A) Spherical statistics analysis of 25 m DEM for Tuaheni South using a 375×375 m roaming window. The analysis has been clipped to the Tuaheni South debris extent (Fig. 2B). B) Areas of eigenvalues below a cut-off value of 0.2 presented semi-transparent with the same colour classification as in A, over the geomorphic map (cf. Fig. 5). Black dotted lines delineate the approximate extent of areas referred to in text, and the general extents of debris bodies T1–T3 are shown.

5.1. Geomorphic constraints on landslide complex development

We propose several explanations for the mode of development of the Tuaheni South landslide complex: mode-1) landslides occur as single, catastrophic events and Tuaheni South is comprised of three discrete failures that produced debris bodies T1–T3, that have not deformed since emplacement; mode-2) Tuaheni South is a retrogressive landslide complex within which failures have occurred in sequence, upslope of an initial failure at the lower end of the landslide. This model implies a progressive younging of event age from the toe towards the head scarp; mode-3) several large failures have occurred and the debris bodies are composed of discrete, stacked (inter-fingered) landslide deposits; or mode-4) following some initial failure(s) that form a debris deposit on the slope, repeated slope failures and debris remobilisation has formed a conveyor-like debris-transport zone (earthflow). The kinematics of these different landslide modes will be reflected in the surface and subsurface morphology of the landslide complex. This morphology can be used to distinguish the model applicable to Tuaheni South.

Longitudinal internal shears occur within the toe area of debris body T3 (Fig. 5), and correlate to a longitudinal zone of large-scale surface roughness in the lower half of the landslide (Fig. 7). This deformation is interpreted as being the result of secondary failure of the landslide body, dismissing the single event emplacement model (mode-1). Additionally, as the subsequent deformation of the landslide deposit is longitudinal, a simple model of a sequence of stacked retrogressive failure bodies (mode-2) with no post-failure deformation is unlikely.

The geometry of surface features, and correlation to deformation at depth, indicates spatially distributed compression and extension across the Tuaheni South landslide debris. In debris body T3,

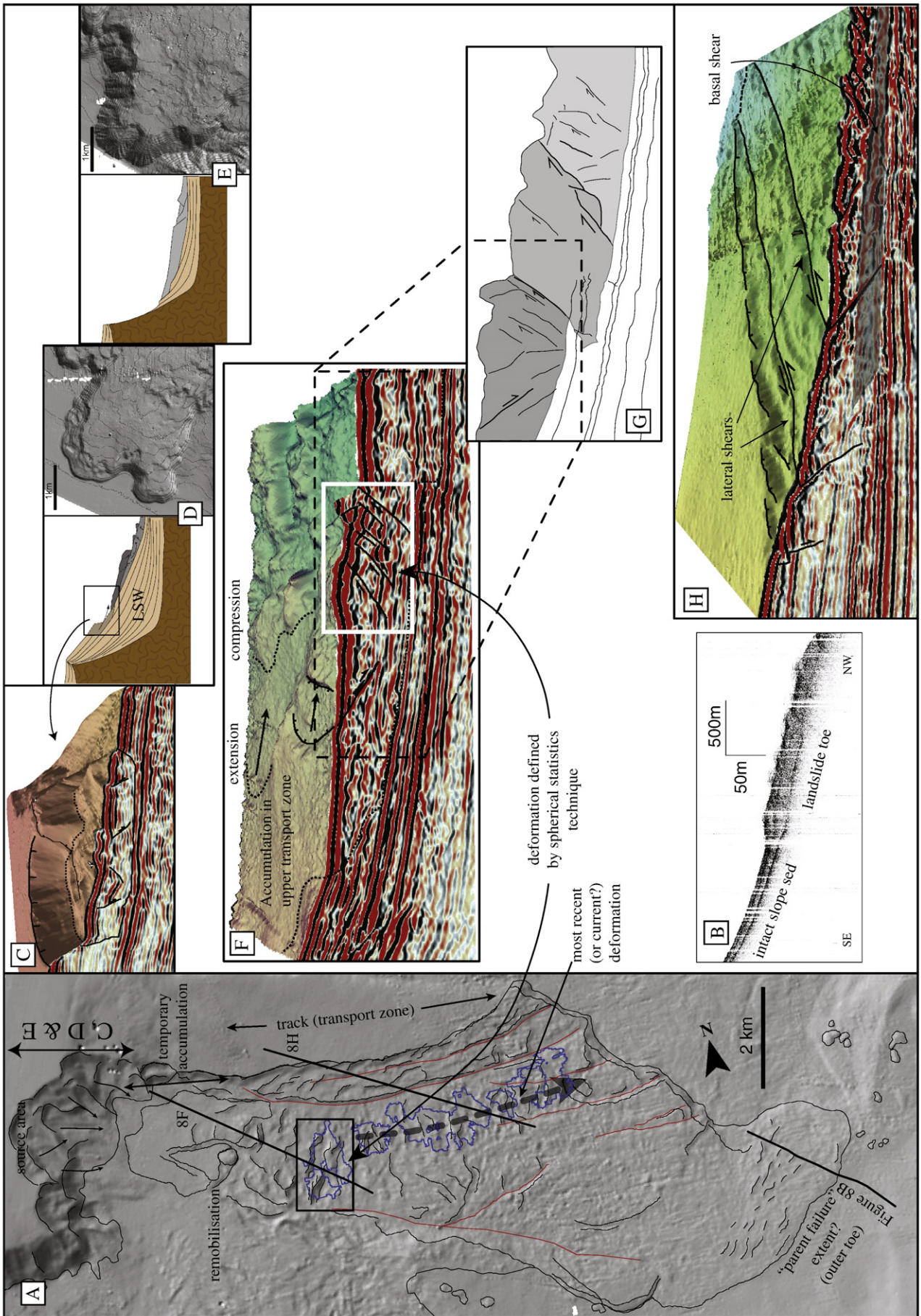
compression occurs near the upper part of the landslide (Figs. 5 and 6B). In a single event failure (mode-1) the upper part of the landslide deposit would be expected to be dominated by extension. The local distribution of compression features indicates secondary reloading from upslope failure. Extension occurs through the lower part of debris body T2 (Fig. 5), interpreted as reflecting a reactivation of landslide debris from the bottom up.

Toe failure scars occur on all debris bodies (T1–T3) indicating secondary failure. Debris body T1 shows a movement direction that is perpendicular to the downslope direction of the large head scarp area above it (“southern head zone” in Fig. 5). This indicates that the most recent deformation in T1 is not related to failure from this southern head zone, but is likely to be as slow, retrogressive displacement of the debris as toe failures perturb the lower boundary stress condition. Whilst this generally fits with a retrogressive-type model (i.e. mode-2), surface morphology suggests slow creeping failure rather than discrete retrogressive failure events.

In addition to the well expressed lateral shears in T2 and T3, which could result from any of the failure modes 1–4 defined above, T3 contains an outer lateral shear on the northern boundary that is interpreted as an abandoned feature. This is both outside the continuous primary lateral shear and sits upslope of it. Volume calculations indicate that $\sim 2 \text{ km}^3$ of material has been removed from the T3 scar area, and the abandoned lateral shear is interpreted as a remnant from earlier landslide activity instrumental in removing this material. The combination of this abandoned feature and the longitudinal movement band are interpreted as reflecting progressive inward stepping of deformation, supporting repeated longitudinal failure at the same site (mode-4).

Despite the extensive landslide deposit, and the multiple arcuate scarps in the head area suggesting numerous (small-scale) failure

Fig. 8. Conceptual model of the anatomy of a submarine earthflow, illustrated in multibeam bathymetric and multichannel seismic reflection data from Tuaheni South debris body T3. A) Geomorphic key map of the earthflow with selected eigenvalue > 0.2 areas from Fig. 7 outlined in blue; B) 3.5 kHz profile across the toe of the interpreted parent failure. The vertical data gaps are a result of acoustic bubble noise below the survey vessel. C) Example of a landslide head zone failure. D and E) Conceptual and multibeam examples of the progressive excavation and eventual depletion of the lowstand wedge. F and G) Remobilisation of material in the accumulation zone and the upslope portion of the transport zone, and H) progressive deformation in the transport zone developing basal and lateral shear geometry, and illustrating the inward stepping movement and entrenchment of the earthflow body and the abandonment of previous lateral shear zones with progressive earthflow development.



events, there is no indication in MCS data for internal partitioning of the landslide debris in Tuaheni South (i.e. there is a lack of internal coherent through going reflectors). If the debris bodies (e.g. T3) were composed of multiple, stacked landslide bodies (mode-3) then these would be likely to be distinguishable in MCS data.

The kinematic features outlined above are consistent with characteristic features of terrestrial earthflows and suggest repeated post-emplacment deformation and material transport within the TLC. This is concluded to be the mechanism for the conveyance of material introduced from the head zone, with the possibly addition of material scavenged from basal erosion, through the landslide transport zone to sediment basins beyond the toe of the landslide.

While we interpret Tuaheni South as a well established earthflow, Tuaheni North shows only localised areas exhibiting features indicating repeated movement. It is clear that the main landslide debris area of Tuaheni North is predominantly affected by comparatively small-scale discrete failures as evidenced by the numerous arcuate scarps in the debris area. There may be several reasons for the difference between the two areas, including: 1) the occurrence of a localised triggering mechanism enabling earthflow mechanics to occur in Tuaheni South (e.g. focused gas/fluid expulsion); 2) the buttressing effect of Tuaheni Ridge to the toe of Tuaheni South forcing the accumulation of landslide debris on the upper slope (note the clear division of the two TLC components by the ~2 km wide unfailed lowstand wedge surface coincident with the northern termination of Tuaheni Ridge, Fig. 2B); 3) the increase in stratigraphic dip to the N/NE affecting the force balance of slope materials (reflected by increased slope gradients to the north, Fig. 2B); 4) a progressive southward evolution of slope failure mode, i.e. the failures in Tuaheni North are a precursor to earthflow development; and 5) a lateral variation in geotechnical properties of the lowstand wedge material (e.g. grainsize, permeability). While further research is required to resolve the apparent contrast in behaviour between Tuaheni South and Tuaheni North; Tuaheni South provides an excellent case study upon which to base a model of submarine earthflow behaviour. In the remainder of this paper we develop a conceptual model for active submarine earthflows as a previously undocumented phenomena, and consider what might be the driving forces behind their mobility.

5.2. Submarine earthflow evolution

Active, or reactivated, subaerial earthflows/mudflows can originate from both large, “parent” landslides, and from local-scale slope failures that subsequently experience deformation from processes such as top-down loading and bottom-up relaxation (Parise, 2003; McKean and Roering, 2004; Borgatti et al., 2006; Comegna et al., 2007). Earthflow-style slope failure is strongly influenced by material properties (strength, grainsize, permeability), site/slope geometry and the nature of stress perturbations on the slope (Baum et al., 2003; Glastonbury and Fell, 2008).

5.2.1. Style of failure within Tuaheni South

Within Tuaheni South we interpret a combination of different earthflow initiation and reactivation processes. In the distal part of T3, failure debris has run up an opposing slope and interacted with existing slope sediments in a compressional manner (Fig. 8A and B), indicating a “parent failure” origin for this component of the landslide complex. Evidence for repeated failure in the T3 source area, as stratigraphically controlled translational block failures (Fig. 8C–E), supports a model of top-down reactivation for debris body T3. Comparison of the southern and northern head zones of Tuaheni South (Fig. 5) indicates that ongoing failures in these areas will deplete the lowstand wedge material (compare Fig. 8D and E), and material supply to the earthflow on the slope below will eventually decline. The occurrence of the two large head zones, interpreted

to have formed through multiple small-scale slope failures, upslope of the landslide complex supports a model of top-down activation of earthflow deformation, at least in the early stages of landslide complex development.

Both of the T1 and T2 debris bodies contain concave downslope fissures and local sediment accumulation that indicate extension (Fig. 5). These landslide bodies both have kilometre-scale failures at the debris toe. This combination of extension through the debris body and lower boundary failure indicates earthflow development by lower boundary destabilisation and bottom-up propagation of displacement. In T1 it is apparent that the contribution of material from the southern head zone to the slope has declined, and deformation has propagated to the northeast through existing debris, likely in response to the stress change at the southern boundary.

Debris body T3 can be used as a case study to evaluate the top-down model of earthflow development and the conveyance of material through the landslide body.

5.2.2. Differential displacement within debris body T3

In debris body T3, the transfer of material from the source area (head scarp) to the toe appears to be dominated by multiple discrete, partitioned remobilisations, rather than by overall creeping movement. From the area of temporary accumulation below the head scarp, material is remobilised into the transport zone (Fig. 8F). Failures are of limited extent and cause compressional deformation within the earthflow body, as is evident in bathymetry and in MCS profiles (Fig. 8A and F). Deformation imaged in MCS data supports a model of failure occurring in sequence down the length of the earthflow body (Fig. 8G). Repeated movement of the landslide debris may cause basal erosion, as indicated by both deflation of the debris body and deformation (incipient failure) of the sequence at the slide base (Fig. 6B). Longitudinally distributed deformation within the transport zone is likely to be a response to perturbed stress states in adjacent material through static loading and the migration of excess pore pressure (c.f. Hutchinson and Bhandari, 1971; Comegna et al., 2007), as well as lower boundary stress relief following toe failure. Pore pressure migration may give rise to an effective pressure wave through the body of the earthflow, accompanied by a localised displacement pulse of the landslide debris.

Longitudinal shears dividing the toe of the earthflow indicates that movement is also partitioned laterally (Fig. 5). If material is being conveyed in “stick-slip” (i.e. punctuated movement) fashion, and inducing localised compressional and/or extensional deformation reflected in surface morphology, then it might be expected that areas currently under compressional stress will stand out as areas of larger scale surface roughness. It is likely that over time, as upslope stresses are relieved in the earthflow body, some “relaxation” will occur along the basal décollement and these larger scale surface features will dissipate. Regional scale spherical statistics analysis (Section 4.1.2) distinguishes different wavelength and amplitude scales of roughness within debris body T3 (Fig. 7). Analysis delineates: 1) a transverse area near the upper end of the transport zone where compression is occurring (cf. Fig. 8A and F); and 2) a discontinuous longitudinal strip down the length of the transport zone which passes between toe shears (Fig. 8A). This area is interpreted as the most recently (or currently) active zone in this earthflow.

5.3. Triggering submarine earthflow movement

Initial mass instability in both terrestrial and submarine hillslopes results from a combination of: 1) slow and sustained (conditioning) and 2) relatively rapid (triggering) processes. The stability of a slope gradually declines under the influence of the sustained processes until it is within a range in which other processes can trigger the ultimate failure (Fig. 9A). On land, the most common longer-term slope-conditioning processes which can both increase the shear stress and

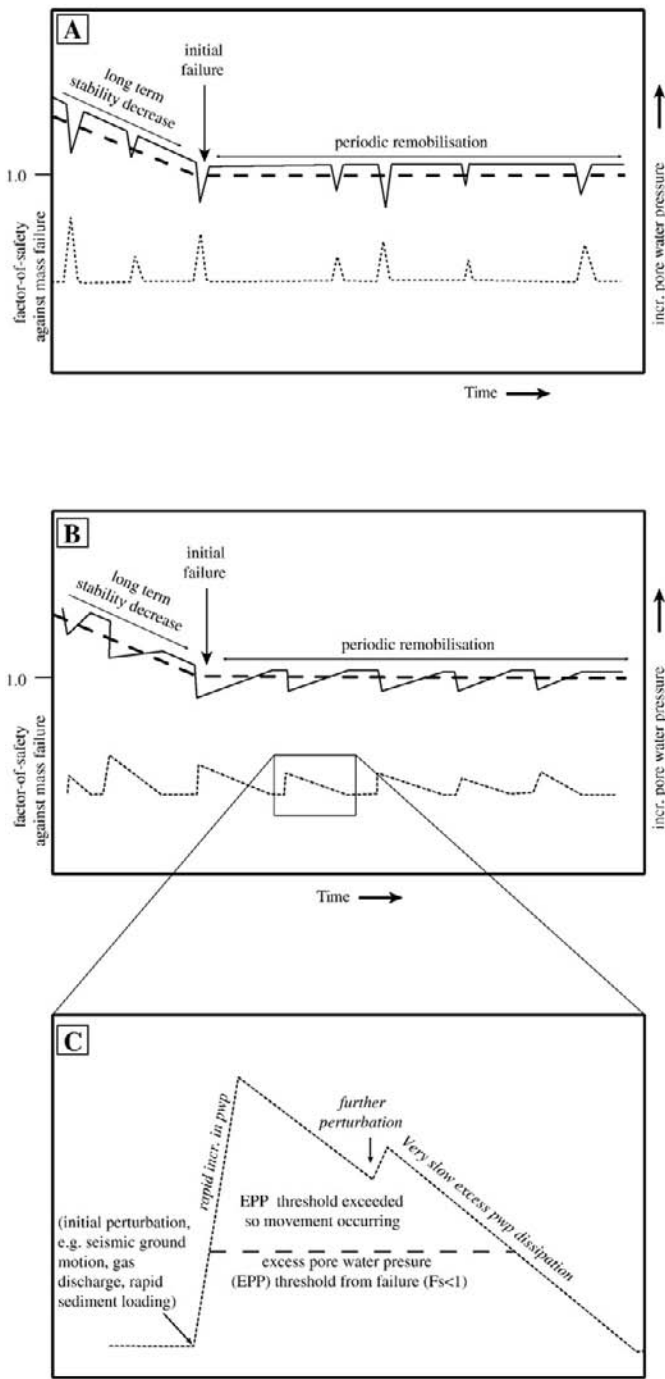


Fig. 9. Conceptual temporal trends of the Factors-of-Safety (Fs) of terrestrial (A) and submarine (B) slopes in response to a combination of long-term slope-weakening processes and final triggering mechanisms. (C) Detail of submarine pore water pressure during a period of slope instability. Dashed lines are the long-term trends of Fs and dotted lines are hypothetical pore pressure trends. Solid lines represent temporal patterns of stability resulting from the combination of long-term weakening of a slope and shorter-term fluctuations due primarily to pore pressure variations. For simplicity the gradual decrease in stability is shown as a linear decline, but in reality it is often more complex.

decrease the shear resistance in a slope include: 1) surcharge loading by material arriving from further upslope, 2) a slow increase in pore water pressure (e.g. associated with progressive surcharge loading), 3) removal of material supporting the toe of a slope (most often by stream erosion), and 4) rock or regolith strength degradation by a variety of physical and chemical processes (e.g. strength loss during earthquakes and other physical and chemical weathering).

In terms of rapid (triggering) processes in terrestrial slope instability, the ultimate trigger is predominantly rainfall. Likewise reactivations of earthflows are controlled by precipitation driven temporal fluctuations of pore water pressures, but also occur by other mechanisms such as snowmelt, earthquake loading and surcharge loading without time for dissipation of consequent elevated pore pressure (Malet et al., 2005; Iverson, 2005; Savage and Wasowski, 2006; Comegna et al., 2007; Calvello et al., 2008). In terrestrial hillslopes these elevated pore pressures often have durations of only hours to months (e.g. Iverson, 2005). Once initiated, terrestrial slides stop when the pore pressure drops below a critical level (shear strength recovers), the material travels onto a gentler slope, or the displaced mass is buttressed by downslope stable material. As noted previously, episodic remobilization of landslide debris is very common in terrestrial earthflows, and typically occurs whenever short-term pore water pressures rise above critical levels (Fig. 9A).

With respect to slope instability, the two most important contrasting differences between subaerial and submarine environments are 1) the effect of wetting and drying as a result of periodic rainfall (submarine slopes are permanently saturated); and 2) the difference in slope gradients (submarine slopes are generally significantly gentler). Despite these differences, most of the long-term processes that can “condition” a submarine slope and bring it to a state of near failure are similar to those for subaerial slopes. Likewise, the processes that ultimately trigger submarine landslides predominantly involve high pore pressures. However, submarine failures are removed from direct precipitation effects and instead high pore pressures are generated by processes such as seismic loading, rapid sedimentation and surcharge loading, and gas expulsion (Hampton et al., 1996) (Fig. 1).

The site for this study is potentially subject to all the triggering processes outlined above, as they are documented to occur elsewhere along the Hikurangi margin, including: high magnitude earthquakes (Reyners, 2000; Barnes et al., 2002); gas hydrates (Pecher et al., 2005); gas seeps (Kvenvolden and Pettinga, 1989; Pettinga, 2003; Klauke et al., in press); and, high sedimentation rates (Orpin et al., 2006; Walsh et al., 2007). We note the presence of “pock mark” features on the slope immediately to the north east of the TLC (Fig. 2B) that may indicate shallow gas or fluid expulsion, and the close proximity of the TLC to earthquake sources such as the Ariel Bank Fault (Fig. 2A). The earthquake potential in this area means that earthquakes will certainly influence slope stability and are likely to play a role in earthflow mobility. The material within which the Tuaheni landslide complex occurs (c.f. Barnes et al., 1991, Section 2) is likely to fit within the range of material properties found for terrestrial earthflows (Fig. 1B), and is characterised as clay rich with a significant component of smectite. Geotechnical testing of comparable materials demonstrates rapid strength degradation under cyclic loading (Barnes et al., 1991). Local slope gradients are relatively steep for submarine slopes at 4–6°, while the landslide debris has a slightly lower gradient (e.g. 2° on debris body T3). Given that the landslides are failing along stratigraphic surfaces, and that surface slopes appear to mimic stratigraphy, this contrast reflects decreasing dips with depth in the lowstand wedge sequence. In comparison to subaerial earthflow debris-surface slope angles, which are typically 7.5–15° (Glastonbury and Fell, 2008), these slope gradients are low but fall within the same order of magnitude.

Perhaps the most significant difference in the mechanical behaviour of submarine vs terrestrial materials, is that elevated pore pressures may decline very slowly in submarine hillslopes relative to the rates in terrestrial settings (Leynaud et al., 2004; Strout and Tjelta, 2005; Sultan et al., 2008). This lower dissipation rate reflects factors including low permeability (fine grained) materials and permanently saturated sediments. As a consequence, submarine landslide debris tends to remain in a metastable condition for long periods of time during which there is an increased potential for remobilization (see

the contrast in temporal pore pressure patterns in terrestrial, Fig. 9A, and submarine slopes, Fig. 9B and C).

One important implication of earthflow-type displacement on submarine slopes is that the low velocity of material movement means slide debris is less likely to transform to a fluidised flow (in comparison to rapid catastrophic failures) and remains in an unstable geometry on the slope. There is also an expected decrease in intrinsic material shear strength during initial failures that leaves the failed mass in a weakened condition (e.g. Skempton, 1985). Periodic reactivation of the earthflow debris leads to retrogressive failure of the head area, as the initial displaced debris moves away from the lower slope of the head scarp. Surcharging of the debris body by retrogressive head scarp failures can generate high pore pressures there with possible remobilization of the older metastable debris by undrained loading of the style discussed by Hutchinson and Bhandari (1971), Iverson (1986, 2005), Comegna et al. (2007) and Bertolini and Pizzolo (2008). While we do not attempt to isolate the specific triggering mechanism for earthflow mobilisation, earthquake ground shaking and gas release are considered the most likely candidates in this study area. Regardless of the specific triggering mechanism we conclude that the metastable condition of the landslide debris body due to sustained excess pore pressure is the critical factor that enables earthflows to develop on submarine slopes.

6. Summary

The field of submarine geomorphology is rapidly advancing, primarily as developments in seafloor imaging technology enable resolution, at unprecedented detail, of the topographic signature of processes affecting submarine slopes. It is no surprise that as we resolve these details, new features are revealed that do not fit traditional models of submarine slope processes. In this study, we have used quantitative morphometric techniques based on high resolution DEM's, combined with interpretation of multichannel seismic reflection data, to analyse patterns of deformation defining the kinematic behaviour of a submarine landslide complex.

This landslide exhibits characteristic features of a slow-moving terrestrial earthflow, contrasting with traditional models of submarine landslide complexes developing from repeated failures mobilising new source material with each event, with the material either accumulating in the same depositional area as slope gradient decreases, or being repetitively flushed through a channelized system. Earthflows are mass movement complexes where landslide debris is repeatedly remobilised along discrete bounding shear surfaces and transported at low velocities, in glacier-like, conveyor-belt style from a source zone in the landslide head area through the main landslide track to the toe where material is either deposited or removed by other processes (e.g. streams). Debris deformation by repeated reactivation of landslide debris bodies is reflected in surface roughness features.

An eigenvalue-based spherical statistics technique delineates a shear-bound elongate area of comparatively larger scale (wavelength and amplitude) surface topography within the Tuaheni landslide complex. This zone is interpreted as the most recently, and possibly the currently, active area of the landslide which is being repeatedly remobilised and is transporting material to the landslide toe. Adjacent shears in the toe area indicate that this is a spatially transient process that defines debris mobility in the lower part of the earthflow.

Movement is inferred to be fundamentally enabled by the ability for excess pore pressures to remain resident in submarine sediment bodies for extended periods of time. Earthflow-style instability is also promoted by the material properties of the extensive, well bedded, undeformed, gently dipping, fine-grained sedimentary sequence deposited on the upper slope. The driving forces that affect initial slope failures and periodic earthflow remobilisation on submarine slopes below the wave base include earthquakes, gas expulsion, and

rapid sediment loading and the Tuaheni landslide complex occurs in an area that is subject to all of these processes. Given the subduction zone setting of the study site, and the numerous active faults mapped in the area, it is reasonable to assume that earthquakes have a significant role in the development of this landslide complex.

While further work is required to definitively show that the Tuaheni landslide complex is an active slow-moving earthflow, the surface and subsurface features observed are consistent with surface features developed in terrestrial earthflows that reflect their kinematic behaviour. The interpretation of submarine landslide complexes as active slow-moving earthflows has wide-ranging implications, including: landslide tsunami hazard analysis (e.g. the large volume of debris on the slope in comparison to the relatively small size of individual catastrophic head scarp failures); continental margin sediment transfer; submarine slope evolution; and design of submarine engineering works. We expect that this process will become widely recognised in other locations, and anticipate that a greater understanding of the driving mechanisms behind repeated remobilisation of submarine earthflow complexes will have a significant contribution to our understanding of submarine slope instability processes.

Acknowledgments

Special thanks to Geoffroy Lamarche for collecting the principle multibeam data set used in this study. The assistance of NIWA technicians Claire Castellazzi, Kevin Mackay, Arne Pallentin and Anne-Laure Verdier is greatly appreciated. Josh Roering assisted with coded spherical statistics routines. This research was partly supported by NZ FRST research contract C01X0702, and by NIWA capability funding. JJM received a Top Achiever Doctoral Scholarship from the New Zealand Tertiary Education Commission. An early draft benefitted from a review by Alan Orpin. The manuscript was much improved following reviews by David Mosher and an anonymous reviewer. Editor David Piper is thanked for his constructive feedback.

References

- Barker, D.H.N., Sutherland, R., Henrys, S., Bannister, S., 2009. Geometry of the Hikurangi subduction thrust and upper plate, North Island, New Zealand. *Geochemical Geophysical Geosystems* 10.
- Barnes, P.M., Ching Cheung, K., Smits, A.P., Almagor, G., Read, S.A.L., Barker, P.R., Froggatt, P.C., 1991. Geotechnical analysis of the Kidnappers Slide, upper continental slope, New Zealand. *Marine Geotechnology* 10, 159–188.
- Barnes, P.M., Nicol, A., Harrison, T., 2002. Late Cenozoic evolution and earthquake potential of an active listric thrust complex above the Hikurangi subduction zone, New Zealand. *Geological Society of America Bulletin* 114 (11), 1379–1405.
- Baum, R.L., Messerich, J., Fleming, R.W., 1998. Surface deformation as a guide to kinematics and three-dimensional shape of slow-moving, clay-rich landslides, Honolulu, Hawaii. *Environmental and Engineering Geoscience* 4 (3), 283–306.
- Baum, R.L., Savage, W., Wasowski, J., 2003. Mechanics of earthflows. *Proceedings of the International Conference FLOWS, Sorrento, Italy*.
- Beavan, J., Tregoning, P., Bevis, M., Kato, T., Meertens, C., 2002. Motion and rigidity of the Pacific Plate and implications for plate boundary deformation. *Journal of Geophysical Research Solid Earth* 107 (B10), 2261.
- Bertolini, G., Pizzolo, M., 2008. Risk assessment strategies for the reactivation of earth flows in the Northern Apennines (Italy). *Engineering Geology* 102 (3–4), 178–192.
- Borgatti, L., Corsini, A., Barbieri, M., Sartini, G., Truffelli, G., Caputo, G., Puglisi, C., 2006. Large reactivated landslides in weak rock masses: a case study from the Northern Apennines (Italy). *Landslides* 3 (2), 115–124.
- Calvello, M., Cascini, L., Sorbino, G., 2008. A numerical procedure for predicting rainfall-induced movements of active landslides along pre-existing slip surfaces. *International Journal for Numerical and Analytical Methods in Geomechanics* 32 (4), 327–351.
- Canals, M., Lastras, G., Urgeles, R., Casamor, J.L., Mienert, J., Cattaneo, A., De Batist, M., Hafidason, H., Imbo, Y., Laberg, J.S., 2004. Slope failure dynamics and impacts from seafloor and shallow sub-seafloor geophysical data: case studies from the COSTA project. *Marine Geology* 213 (1–4), 9–72.
- Carter, L., Manighetti, B., 2006. Glacial/interglacial control of terrigenous and biogenic fluxes in the deep ocean off a high input, collisional margin: a 139 kyr-record from New Zealand. *Marine Geology* 226, 307–322.
- Comegna, L., Picarelli, L., Urciuoli, G., 2007. The mechanics of mudslides as a cyclic undrained-drained process. *Landslides* 4 (3), 217–232.

- Cruden, D.M., Varnes, D.J., 1996. Landslide types and processes. In: Turner, A.K., Schuster, R.L. (Eds.), *Landslides: Investigation and Mitigation*. National Academy Press, Washington, D.C., p. 673.
- Evans, D., Harrison, Z., Shannon, P.M., Laberg, J.S., Nielsen, T., Ayers, S., Holmes, R., Houlter, R.J., Lindberg, B., Hafliðason, H., 2005. Palaeoslides and other mass failures of Pliocene to Pleistocene age along the Atlantic continental margin of NW Europe. *Marine and Petroleum Geology* 22 (9–10), 1131–1148.
- Fleming, R.W., Johnson, A.M., 1989. Structures associated with strike-slip faults that bound landslide elements. *Engineering Geology* 27 (1–4), 39–114.
- Gee, M.J.R., Uy, H.S., Warren, J., Morley, C.K., Lambiase, J.J., 2007. The Brunei slide: a giant submarine landslide on the North West Borneo Margin revealed by 3D seismic data. *Marine Geology* 246 (1), 9–23.
- Glastonbury, J., Fell, R., 2008. Geotechnical characteristics of large slow, very slow, and extremely slow landslides. *Canadian Geotechnical Journal* 45 (7), 984–1005.
- Glenn, N.F., Streutker, D.R., Chadwick, D.J., Thackray, G.D., Dorsch, S.J., 2006. Analysis of LIDAR-derived topographic information for characterizing and differentiating landslide morphology and activity. *Geomorphology* 73 (1–2), 131–148.
- Greene, H.G., Murai, L.Y., Watts, P., Maher, N.A., Fisher, M.A., Paull, C.E., Eichhubl, P., 2006. Submarine landslides in the Santa Barbara Channel as potential tsunami sources. *Natural Hazards and Earth System Science* 6 (1), 63–88.
- Hampton, M.A., Lee, H.J., Locat, J., 1996. Submarine landslides. *Reviews of Geophysics* 34, 33–59.
- Hobson, R.D., 1972. Surface roughness in topography: a quantitative approach. *Spatial Analysis in Geomorphology* 221–245.
- Hungr, O., Evans, S.G., Bovis, M.J., Hutchinson, J.N., 2001. A review of the classification of landslides of the flow type. *Environmental and Engineering Geoscience* 7 (3), 221–238.
- Hutchinson, J.N., 1988. General report: morphological and geotechnical parameters of landslides in relation to geology and hydrogeology. *landslides: Proc. 5th Symposium, Lausanne, vol. 1*, pp. 3–35.
- Hutchinson, J.N., Bhandari, R.K., 1971. Undrained loading, a fundamental mechanism of mudflows and other mass movements. *Geotechnique* 21 (4), 353–358.
- Iverson, R.M., 1986. Unsteady, nonuniform landslide motion: 1 Theoretical dynamics and the steady datum state. *Journal of Geology* 94 (1), 1–15.
- Iverson, R.M., 2005. Regulation of landslide motion by dilatancy and pore pressure feedback. *Journal of Geophysical Research F: Earth Surface* 110 (2).
- Klaucke, I., Weinrebe, W., Petersen, C.J., Bowden, D., in press. Temporal variability of gas seeps offshore New Zealand: multi-frequency geoaoustic imaging of the Wairarapa area, Hikurangi margin. *Marine Geology*. doi:10.1016/j.margeo.2009.02.009.
- Kvenvolden, K.A., Pettinga, J.R., 1989. Hydrocarbon gas seeps of the convergent Hikurangi Margin, North Island, New Zealand. *Marine and Petroleum Geology* 6, 2–8.
- Lewis, K., Lallemand, S., Carter, L., 2004. Collapse in a Quaternary shelf basin off East Cape, New Zealand: evidence for passage of a subducted seamount inboard of the Ruatoria giant avalanche. *New Zealand Journal of Geology and Geophysics* 47, 415–429.
- Leynaud, D., Mienert, J., Nadim, F., 2004. Slope stability assessment of the Helland Hansen area offshore the mid-Norwegian margin. *Marine Geology* 213 (1–4), 457–480.
- Locat, J., Lee, H.J., 2002. Submarine landslides: advances and challenges. *Canadian Geotechnical Journal* 39 (1), 193–213.
- Malet, J.P., van Asch, T.W.J., van Beek, R., Maquaire, O., 2005. Forecasting the behaviour of complex landslides with a spatially distributed hydrological model. *Natural Hazards and Earth System Science* 5 (1), 71–85.
- McKean, J., Roering, J., 2004. Objective landslide detection and surface morphology mapping using high-resolution airborne laser altimetry. *Geomorphology* 57 (3–4), 331–351.
- Micallef, A., Berndt, C., Masson, D.G., Stow, D.A.V., 2007a. A technique for the morphological characterization of submarine landscapes as exemplified by debris flows of the Storegga Slide. *Journal of Geophysical Research F: Earth Surface* 112 (2).
- Micallef, A., Masson, D.G., Berndt, C., Stow, D.A.V., 2007b. Morphology and mechanics of submarine spreading: a case study from the Storegga Slide. *Journal of Geophysical Research F: Earth Surface* 112 (3).
- Mulder, T., Cochonat, P., 1996. Classification of offshore mass movements. *Journal of Sedimentary Research* 66, 43–57.
- Multiwave, 2005. 05CM 2D Seismic survey, offshore East Coast - North Island, New Zealand. Unpublished openfile petroleum report 3136. Ministry of Economic Development, Wellington.
- Orpin, A.R., Alexander, C., Carter, L., Kuehl, S., Walsh, J.P., 2006. Temporal and spatial complexity in post-glacial sedimentation on the tectonically active, Poverty Bay continental margin of New Zealand. *Continental Shelf Research* 26 (17–18), 2205–2224.
- Paquet, F., Proust, J.-N., Barnes, P.M., Pettinga, J.R., 2009. Inner-forearc sequence architecture in response to climatic and tectonic forcing since 150 Ka: Hawke's Bay, New Zealand. *Journal of Sedimentary Research* 79, 97–124.
- Parise, M., 2003. Observation of surface features on an active landslide, and implications for understanding its history of movement. *Natural Hazards and Earth System Science* 3 (6), 569–580.
- Pecher, I.A., Henrys, S.A., Ellis, S., Chiswell, S.M., Kukowski, N., 2005. Erosion of the seafloor at the top of the gas hydrate stability zone on the Hikurangi Margin, New Zealand. *Geophysical Research Letters* 32 (24), 1–4.
- Pettinga, J.R., 2003. Mud volcano eruption within the emergent accretionary Hikurangi margin, southern Hawke's Bay, New Zealand. *New Zealand Journal of Geology & Geophysics* 46, 107–121.
- Picarelli, L., Urciuoli, G., Ramondini, M., Comegna, L., 2005. Main features of mudslides in tectonised highly fissured clay shales. *Landslides* 2 (1), 15–30.
- Posamentier, H.W., Vail, P.R., 1988. Eustatic controls on clastic deposition II – sequence and systems tract models. In: Wilgus, C.K., Posamentier, H., Ross, C.A., Kendall, C.G.S. (Eds.), *Sea-level Changes: an Integrated Approach*. Society of Economic Paleontologists and Mineralogists, Special Publication, pp. 125–154.
- Reyners, M.E., 2000. Quantifying the hazard of large subduction thrust earthquakes in Hawke's Bay. *Bulletin of the New Zealand National Society for Earthquake Engineering* 33 (4), 477–483.
- Savage, W., Wasowski, J., 2006. A plastic flow model for the Acquara-Vadoncello landslide in Senerchia, Southern Italy. *Engineering Geology* 83 (1–3), 4–21.
- Skempton, A.W., 1985. Residual strength of clays in landslides, folded strata and the laboratory. *Geotechnique* 35 (1), 3–18.
- Stirling, M.W., McVerry, G.H., Berryman, K.R., 2002. A new seismic hazard model for New Zealand. *Bulletin. Seismological Society of America* 92 (5), 1878–1903.
- Strout, J.M., Tjelta, T.I., 2005. In situ pore pressures: what is their significance and how can they be reliably measured? *Marine and Petroleum Geology* 22 (1–2 SPEC. ISS), 275–285.
- Sultan, N., Cattaneo, A., Sibuet, J.C., Schneider, J.L., 2008. Deep sea in situ excess pore pressure and sediment deformation off NW Sumatra and its relation with the December 26, 2004 Great Sumatra–Andaman Earthquake. *International Journal of Earth Sciences* 1–15.
- Varnes, D.J., 1978. Landslide types and processes. In: Schuster, R.L., Krizek, R.J. (Eds.), *Special Report 176: Landslides: Analysis and Control*. Transportation Research Board, Washington DC, pp. 11–33.
- Walsh, J.P., Alexander, C.R., Gerber, T., Orpin, A.R., Summers, B.W., 2007. The demise of a submarine canyon? Evidence for highstand infilling on the Waipaoa River continental margin, New Zealand. *Geophysical Research Letters* 34 (L20606).
- Woodcock, N.H., 1977. Specification of fabric shapes using an eigenvalue method. *Geological Society of America Bulletin* 88, 1231–1236.